

# Observations of low-frequency acoustic-to-seismic coupling in the summer and winter<sup>a)</sup>

Donald G. Albert

*U.S. Army Cold Regions Research and Engineering Laboratory, 72 Lyme Road, Hanover, New Hampshire 03755-1290*

John A. Orcutt

*Institute of Geophysics and Planetary Physics (A-025), Scripps Institute of Oceanography, La Jolla, California 92093*

(Received 25 September 1988; accepted for publication 23 March 1989)

Experiments were conducted at a site in northern Vermont to investigate low-energy acoustic-to-seismic coupling in the 5- to 500-Hz frequency band for propagation distances between 1 and 274 m. Pistol shots were used as the source of the acoustic waves, with geophones and microphones serving as the receivers. The strongest coupling into the ground occurred as the air wave passed, with measured ratios of about 7 and  $6 \times 10^{-6} \text{ m s}^{-1} \text{ Pa}^{-1}$  in the summer and winter, respectively. Compressional waves induced in the ground immediately under the source were observed as first arrivals, since they travel at the higher subsurface seismic wave velocity, but their amplitudes were one to two orders of magnitude lower than those of the later-arriving air wave. A comparison of the summer and winter recordings revealed a number of effects caused by the introduction of a 0.25-m-thick snow cover. The peak amplitude of the seismic arrival induced by the passage of the acoustic wave was more strongly attenuated in the winter, with a decay rate proportional to  $r^{-1.9}$  vs  $r^{-1.2}$  in the summer. These observed decay rates are shown to agree with the calculated absorption of energy from the airborne acoustic wave by the finite impedance ground surface. The snow cover also produced a strong waveguide effect that enhanced the low-frequency air-coupled Rayleigh waves and considerably changed the appearance of the received waveforms.

PACS numbers: 43.28.Fp, 43.28.Dm, 43.40.Ph

## INTRODUCTION

Acoustic-to-seismic coupling can have large effects on the performance of sensor systems that utilize ground motion to detect intruders or to locate targets, and thus has been the subject of much recent study. Early investigations, which date back to the 1930s, focused on air-coupled Rayleigh waves or flexural waves that can be observed at very large ranges (see Refs. 1 and 2). Recently, work has been done on coupling at shorter ranges. Researchers<sup>3-7</sup> developed probe microphones that can be inserted into the soil and, using continuous sound sources, they showed that the coupling was mainly a local phenomenon, with the seismic waves being induced by the passage of the air wave directly over the sensors, in agreement with the earlier work. Body waves as well as surface waves have been detected from impulsive sources in the air.<sup>8-10</sup>

A 0.70-m-thick snow cover can strongly attenuate the coupling,<sup>11</sup> while enhanced coupling has been observed when a thin snow layer was present.<sup>8</sup> Increases and decreases in the coupling through various snow layers have been measured, which could not be explained by a simple dependence on layer thickness.<sup>12</sup>

This paper presents measurements undertaken to investigate acoustic-to-seismic coupling under summer and win-

ter conditions at a site in northern Vermont. By using an impulsive rather than a continuous source, these measurements allow the various wave types to be identified and examined individually. We focus our attention primarily on the changes that result from the introduction of a snow layer.

## I. EXPERIMENTAL PROCEDURE

The experiments were conducted at the Known Distance Firing Range of the Vermont National Guard's Camp Ethan Allen Training Center in Jericho, Vermont (Fig. 1). The test site is located approximately 17 km east of Burlington, Vermont, at 44°27.5'N, 72°55'W, and is about 240 m above sea level. The relatively flat site allowed propagation ranges of up to a few hundred meters to be used. Controlled access to the site ensured that the snow cover was undisturbed.

A Geosource DSS-10A seismic recording system was used to sample 24 data channels at 2000 samples/s. This recording system has a flat frequency response from 3 to 500 Hz and a dynamic range of 90 dB. Occasionally, a 60-Hz notch filter was necessary, but other filtering was avoided during the measurements so that the recorded bandwidth was as wide as possible.

For most of the receiver channels, Mark Products L-15B vertical component geophones with a natural frequency of 4.5 Hz and a sensitivity of  $32 \text{ V/m s}^{-1}$  measured the particle velocity of the soil or snow. Horizontal component geophones of the same type were also used to assist in identi-

<sup>a)</sup> An earlier version of this paper was presented at the 114th Meeting of the Acoustical Society of America [J. Acoust. Soc. Am. Suppl. 1 82, S77 (1987)].

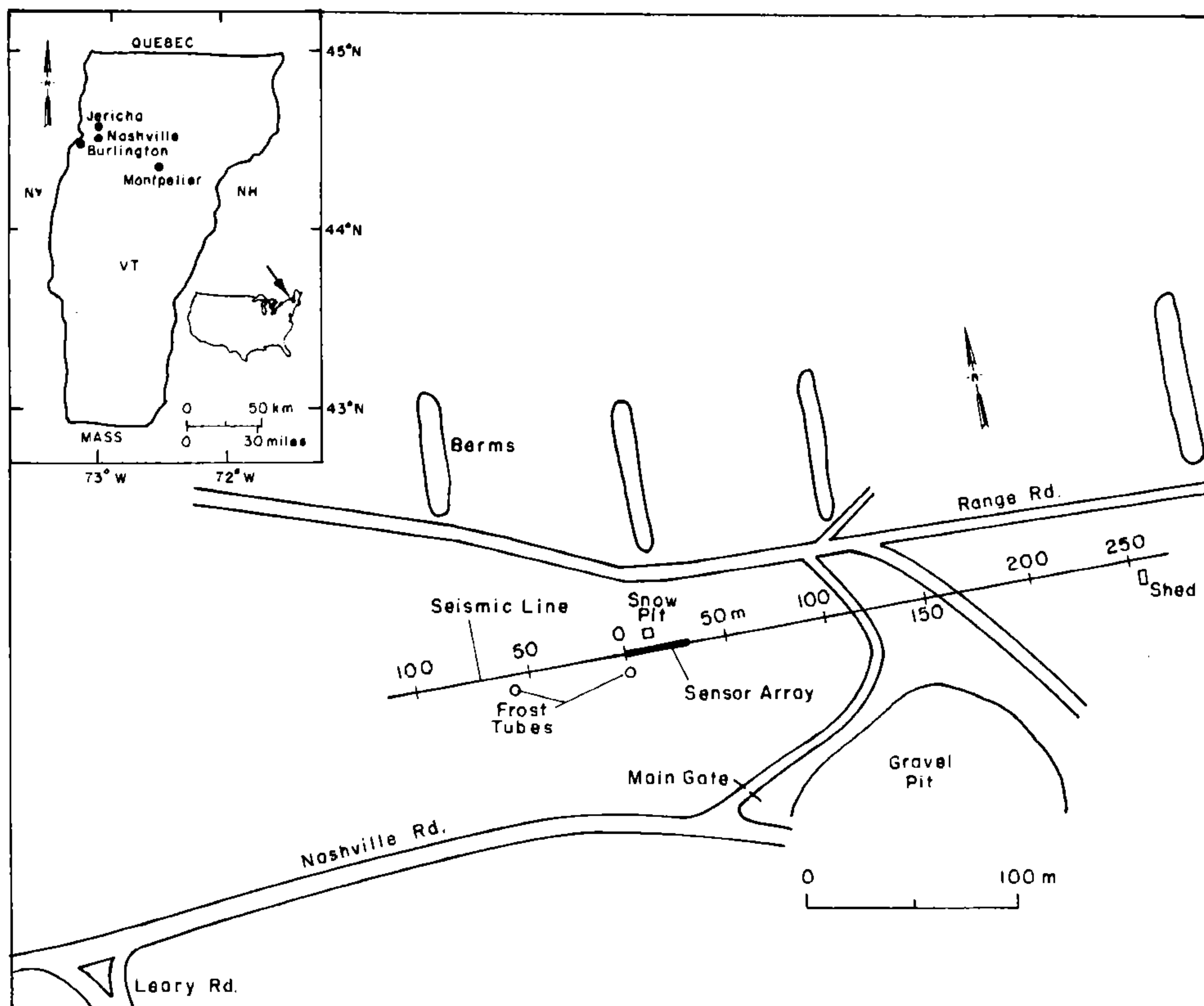


FIG. 1. Location map. The site of the experiments was Camp Ethan Allen, located between the villages of Jericho and Nashville, Vermont.

fying the wave types and to allow the particle motion to be determined. These geophones were held in place in the soil or snow by a 75-mm-long spike attached to the case. Globe 100C low-frequency capacitor microphones with a sensitivity of 2 V/Pa were placed on the surface or on small wooden platforms 0.5 m high and were covered with 0.6-m-diam screens to reduce wind noise. For the acoustic source, a .45 caliber pistol was held horizontally 1 m above the surface and blank shots were fired toward the sensors.

Figure 2 shows schematic diagrams of the receiver arrays used in the summer and winter. The geophones were installed at the ground or snow surface with at least one geophone every 3 m. At one location, a vertical component geophone was buried beneath the ground surface, but its depth was limited to 0.33 m in the summer and 0.25 m in the winter by the difficulty of digging through the gravelly soil. Microphones were installed at the ground surface and at a

height of 0.5 m at two locations in the array. A single subsurface microphone was also installed, but noise problems prevented any useful data from being obtained. The vertical component geophones at the ground surface and buried in the soil at horizontal distance 0 m were installed 2 months before the winter measurements when there was no snow cover. Attempts to find a second pair of geophones at a distance of 18 m were unsuccessful and were responsible for the void in the snow cover depicted in Fig. 2. Care was taken to minimize the disturbance of the snow cover when the other sensors were installed in the winter.

The arrangement of sources and receivers was designed to allow the different waves to be observed separately so that their velocities and amplitudes could be accurately determined. Because the receiver array required a few hours to install, it remained in a fixed location for each particular experiment while the position of the source was varied. A

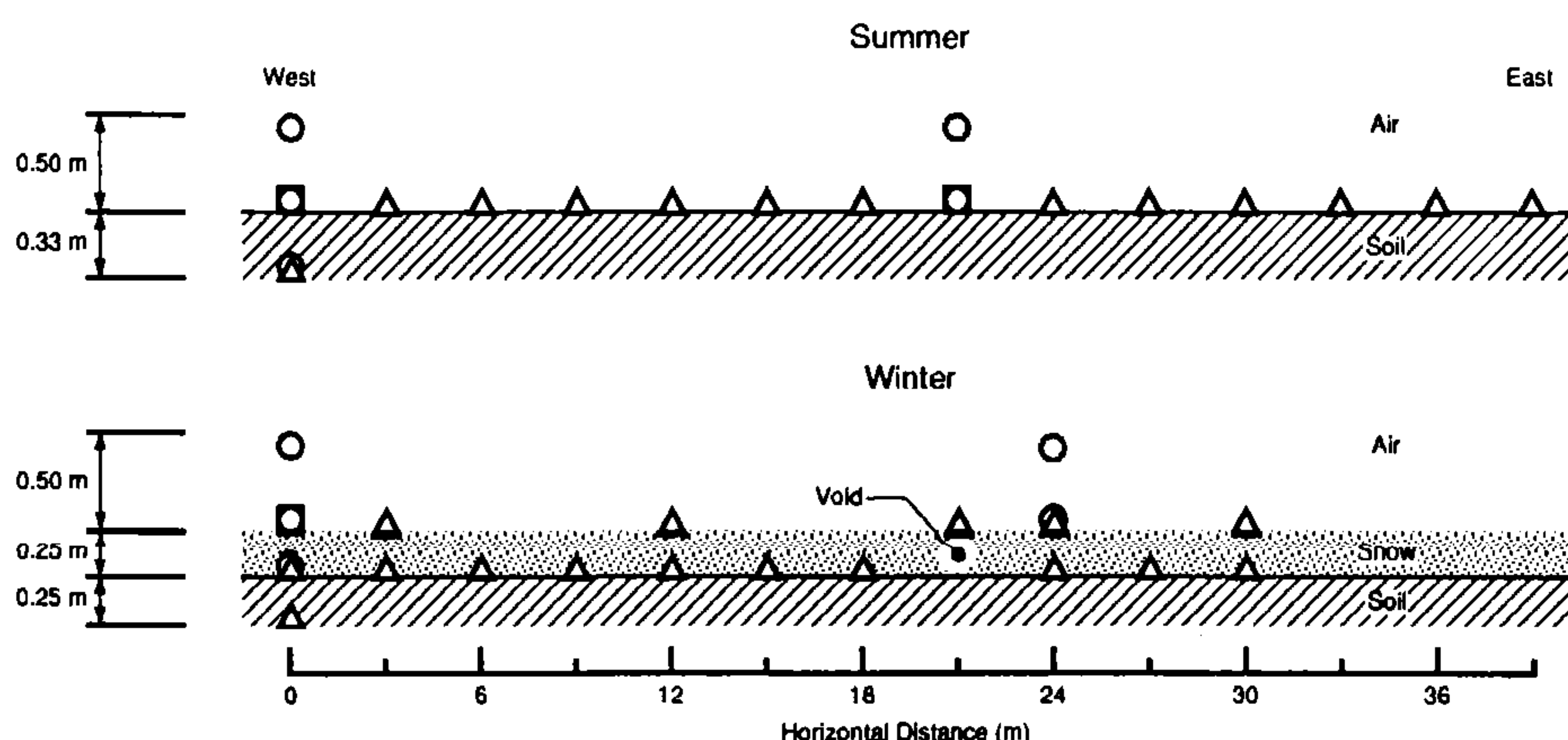


FIG. 2. Schematic cross-sectional view of the sensor arrays used in the summer (top) and winter (bottom) experiments. A triangle denotes the location of a vertical component geophone, a square locates a three-component geophone (actually two separate horizontal component geophones and a vertical component geophone), and a circle denotes a microphone.

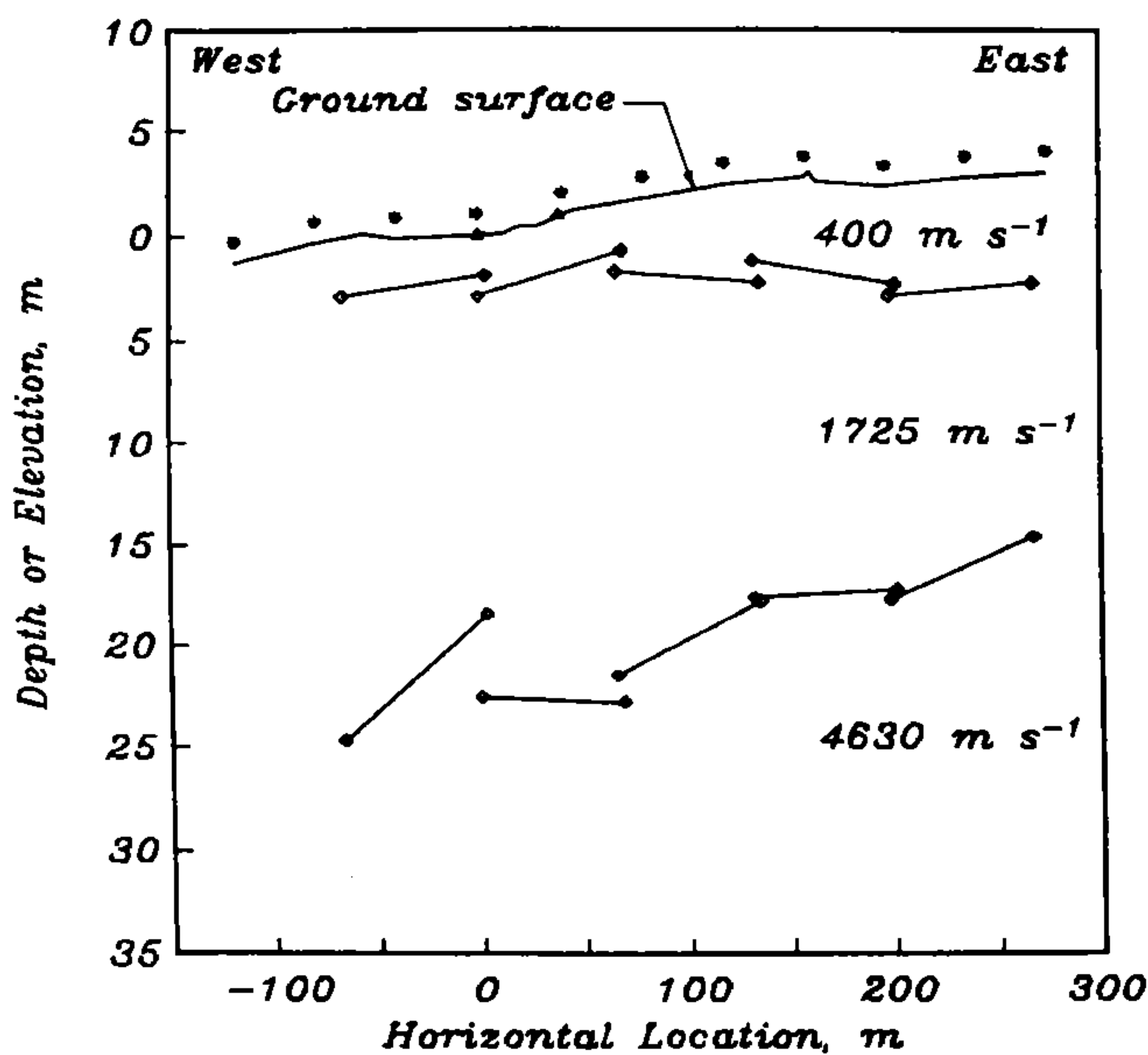


FIG. 3. Results of *P*-wave refraction measurements. Five separate receiver arrays were used; the resulting depths from intercept time analysis are denoted with diamonds. Triangles mark the ends of the receiver arrays and asterisks the source locations for the acoustic-to-seismic coupling experiments. The vertical to horizontal exaggeration is 10:1.

number of recordings were made with the source at one end of the receiver array; then the source was moved away at intervals slightly less than the array length (to provide some overlap) and the measurements were repeated. This procedure allowed the entire wave field to be recorded at a distance interval of 3 m, with maximum propagation ranges of 157 m from the west and 274 m from the east. Since different waves travel at different velocities, they can be observed separating from one another as the propagation distance increases. From the recorded data, travel time versus distance and amplitude versus distance curves can be constructed to determine the velocity and the amplitude decay of the waves. Comparison of the amplitude of the signals from geophones at the same location but at different depths allows the attenuation constants of the snow and soil to be estimated.

## II. SITE CHARACTERIZATION

Seismic refraction techniques were used during the summer to determine the compressional (*P*) and shear (*S*) wave velocity structure of the site. These measurements reveal

typically low *P*- and *S*-wave surface soil velocities of 200 and 60 m s<sup>-1</sup>, respectively. The shear wave velocity increased to 160 m s<sup>-1</sup> at a depth of 0.2 m, to 360 m s<sup>-1</sup> at 1.5 m, and to 2900 m s<sup>-1</sup> at 24-m depth beneath the 39-m-long receiver array. The more extensive *P*-wave measurements, conducted over a 344-m line, indicate a nearly horizontal layer with a velocity of 1725 m s<sup>-1</sup> at 4-m depth, identified as the water table. The velocities range from 3900–5700 m s<sup>-1</sup> (mean 4630, standard deviation 710 m s<sup>-1</sup> for six determinations) beginning at a depth of 15 m at the eastern end of the site, and at 25-m depth at the western end (Fig. 3). These velocities indicate that the upper 15 to 25 m consist of unconsolidated soils, becoming saturated at 4-m depth, with the basement rock below. Note that the shear wave velocity is unaffected by the saturation of the soil.

Stewart and McClintock<sup>13</sup> have indicated that surface soils in this area have been mapped as outwash deposits, i.e., glaciofluvial gravels, with a possible thin covering of postglacial alluvium, and this agrees with a number of shallow soil samples that were collected during the summer. Laboratory analysis showed the soils to consist of gravel–sand–silt mixtures or of silty sands with densities around 1700 kg m<sup>-3</sup>. The bedrock geology of the site belongs to the Pinnacle formation, a lower Cambrian formation of the Camel's Hump group, composed of metamorphosed (albite to chlorite) shistose graywacke.<sup>14</sup>

The summer recordings were made on 18 and 19 August 1986, both partly cloudy, hot (28 °C), and humid days. The variable winds were estimated to range between speeds of 2–3 m s<sup>-1</sup>, blowing across the acoustic propagation path from the north, and causing a neutral (zero gradient) temperature profile. The measured speed of sound in the air was 346 m s<sup>-1</sup>.

The winter experiments took place on 16 January 1986, with a snow cover of about 0.25 m and a thin (0.03-m) layer of frozen soil present at the site. Five distinct layers were observed in the snowpack, with measured densities from 190 to 290 kg m<sup>-3</sup>, and crystal sizes ranging from 0.1–2 mm (Table I). The winds remained nearly calm throughout the day, with clear skies and air temperatures between –8 and –3.5 °C. The measured speed of sound in air was lower than in the summer, 329 m s<sup>-1</sup>, because of the lower temperatures. The air temperature was lower near the cold snow cover, and increased with height, producing an inversion (positive temperature gradient).

TABLE I. Snow layer profile of 26 January 1986, 1530 hours.

Layer	Thickness (mm)	Density (kg m <sup>-3</sup> )	Temperature (°C)	Hardness index	Crystal size (mm)	Crystal type
1	40	192	–10	2.5	0.1	windblown
2	30	198	–5	450	0.1–0.3	granular and fragments
3	40	198	–6	25	0.5	hexagonal and columns
4	120	288	–2	250	1–2	hexagonal
5	20	(900)	–3	3500	...	ice lens

A leveling survey of the site revealed a maximum elevation change of 4.27 m over the 392-m line of sources and receivers. (For Vermont, that's considered flat!) The site generally sloped upwards from west to east, with some irregularities. All of the receiver locations were within 0.95 m in elevation.

### III. OBSERVATIONS

Figures 4 and 5 show typical examples of the observed signal output from vertical component geophones in the summer and winter, and display how the signals change as they penetrate a short distance beneath the surface. The source is a .45 caliber blank pistol shot 1 m above the ground surface. The large amplitude arrival near 0.2 s in Fig. 4 and 0.8 s in Fig. 5 is the seismic pulse induced by the passage of the acoustic wave from the shot. It is this seismic arrival, which travels primarily through the atmosphere and couples locally into the ground, that we call the *air wave* in this paper. In the summer, the initial soil particle motion is downward and is followed by rapid, high-frequency oscillations. In the winter, the air wave is greatly reduced in amplitude and is followed by a low-frequency wavetrain that is not observed in the summer. The air wave is delayed in the winter relative to the summer arrival time because of the temperature-induced change of the speed of sound in air. The ratio of the summer and winter pulse amplitudes is about 8:1. These differences between summer and winter amplitudes persist at all the propagation ranges and are caused by the different atmospheric sound-speed profiles and the presence of the snow cover.

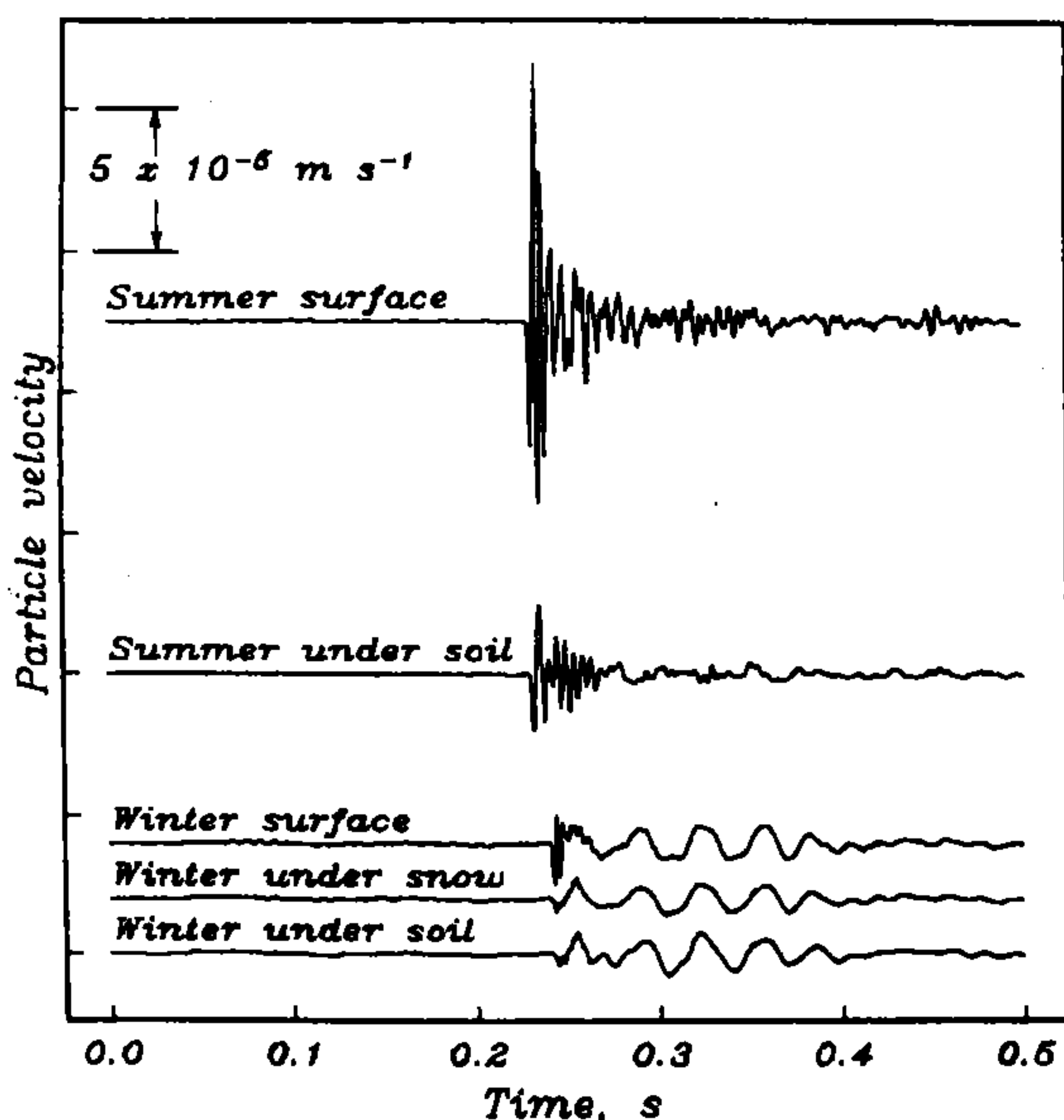


FIG. 4. True amplitude comparison of vertical component geophone recordings in summer and winter. The source was a 0.45 blank pistol shot from a location 1 m above the snow and 79 m to the east of the geophones, which were located at the horizontal axis origin shown in Figs. 2 and 3. The source and receiver locations are identical for all traces. In the summer, the surface geophone was on the ground surface, while in the winter the surface geophone was on the top of the 0.25-m-thick snow cover. The buried geophone was 0.33 m deep in the summer and 0.25 m below the ground surface in the winter.

The ratio of induced particle velocity to incident pressure was determined from peak values of the air wave recorded by collocated vertical component surface geophones and surface microphones. In the summer, 64 separate shots or stacked shots gave a mean ratio of  $6.9 \pm 0.4 \times 10^{-6} \text{ m s}^{-1} \text{ Pa}^{-1}$  with 95% confidence interval bounds. In the winter, 54 individual measurements yielded a mean ratio of  $5.9 \pm 0.6 \times 10^{-6} \text{ m s}^{-1} \text{ Pa}^{-1}$ . Since all the measurements were at grazing angles of incidence, no range dependence of the ratio was observed. These ratios are similar to values obtained previously for other soil types. Using continuous sources, researchers have reported peak values (at a single frequency) of  $5 \times 10^{-6}$  to  $10 \times 10^{-6} \text{ m s}^{-1} \text{ Pa}^{-1}$  for silt loam,<sup>4</sup>  $8 \times 10^{-6}$  for loess,<sup>5</sup> and  $13 \times 10^{-6}$  for dredged sand.<sup>5</sup> Using an impulsive source, a value of  $2 \times 10^{-6} \text{ m s}^{-1} \text{ Pa}^{-1}$  has been reported for sandy soil.<sup>15</sup>

The dimensionless energy density ratio ER of the seismic to the acoustic waves can be estimated using

$$ER = \rho_s v^2 / (p^2 / \rho_a c^2) = \rho_s \rho_a c^2 v^2 / p^2, \quad (1)$$

where  $\rho$  is the density in  $\text{kg m}^{-3}$ ,  $c$  is the speed of sound in air in  $\text{m s}^{-1}$ ,  $v$  is the particle velocity in the solid in  $\text{m s}^{-1}$ ,  $p$  is the pressure in air in Pa, and the subscripts  $a$  and  $s$  refer to air and solid (soil or snow), respectively. Assuming  $1.2 \text{ kg m}^{-3}$  for the density of air and substituting the measured values of  $\rho_s$ ,  $c$ , and  $v/p$  (the average seismic to acoustic ratio) into Eq. (1) give energy ratios of 1.2% and 0.09% in the summer and winter. Since  $v/p$  is nearly constant for the two seasons, the difference in energy transmitted arises mainly from the order of magnitude difference between the soil and snow densities.

By comparing the signals from the surface and buried geophones, their decay as they penetrate beneath the surface can be determined. For example, the signals displayed in both Figs. 4 and 5 show that in the summer the large amplitude air wave is reduced by a factor of 2 as it penetrates from the surface to 0.33-m depth. In the winter, the air wave again

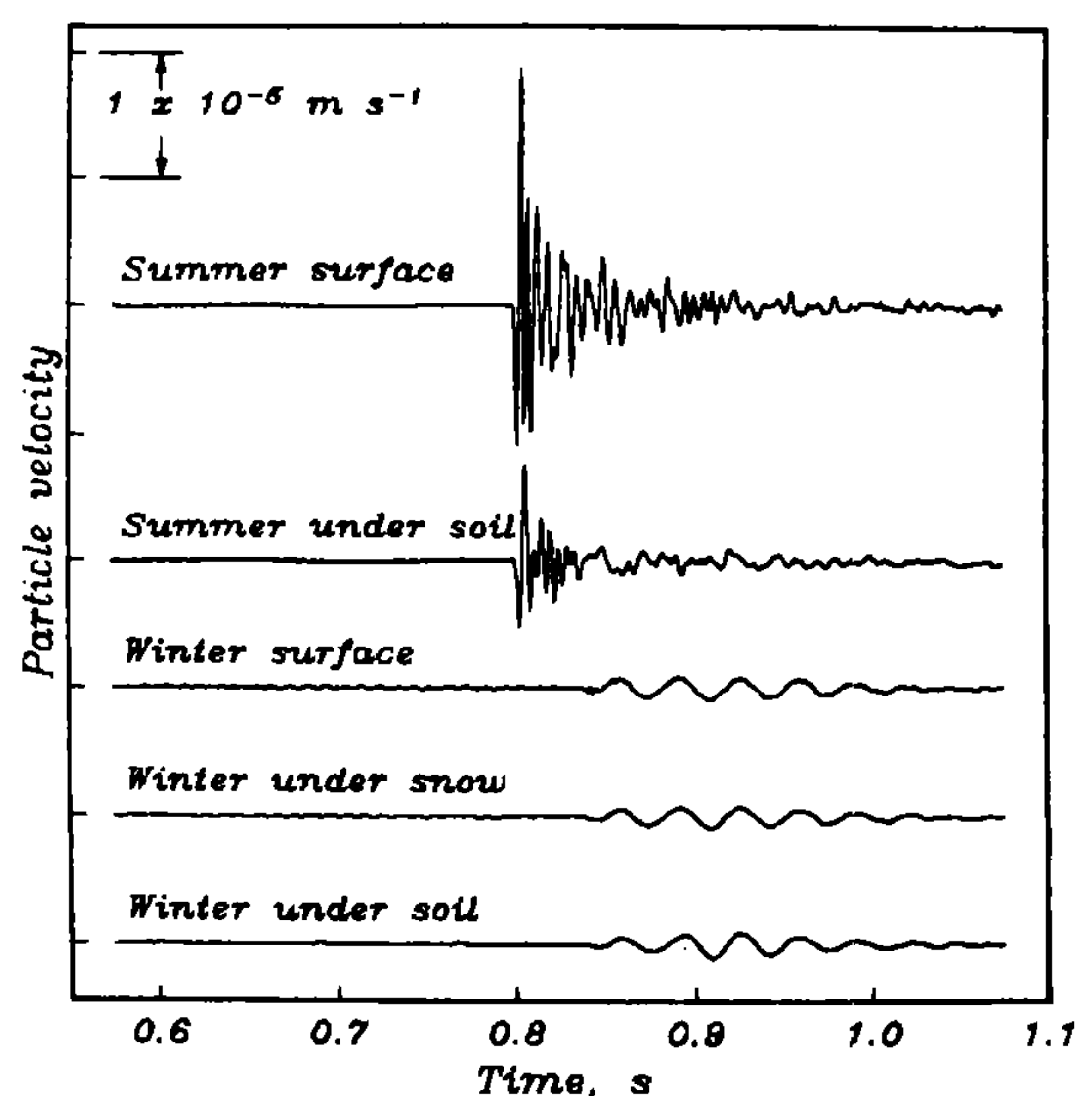


FIG. 5. True amplitude comparison of vertical component geophone recordings in summer and winter, for ten firings from a position located 274 m to the east of the geophones. The receivers are identical to those in Fig. 4.

is strongly attenuated, dropping by a factor of 3 in passing from the surface through 0.25 m of snow, and by a factor of 4 in passing through the snow and 0.25 m of soil. Because the air wave is at grazing incidence in these examples, the attenuation does not depend on the propagation range. The decay in amplitude is caused by mechanical losses in the soil and snow, i.e., the conversion of elastic energy to heat. The attenuation coefficient  $\alpha$ , defined by

$$A(z) = A(0)e^{-\alpha z}, \quad (2)$$

where  $z$  is depth in m,  $A(z)$  is the amplitude in  $\text{m s}^{-1}$  of geophone at depth  $z$ , and  $A(0)$  is the amplitude at the surface, was determined from all of the measured amplitudes for propagation ranges of 40 m or greater (Table II). For both the soil and the snow,  $\alpha$  has a value of around  $2 \text{ m}^{-1}$ . The actual path length  $h$  through the snow or soil should be used in place of the vertical depth  $z$  in Eq. (2), but this path length depends on the subsurface velocity (which is hard to measure accurately) via the equation

$$h = z[1 - (c_s/c)^2]^{-1/2}, \quad (3)$$

where  $c_s$  and  $c$  are the wave velocities in the subsurface material and in air. For the soil, the measured velocity of  $200 \text{ m s}^{-1}$  indicates that  $h = 1.26z$ ; i.e., the two values of  $\alpha$  for soil in Table II are about 25% too high. For snow, the estimated velocity of  $100 \text{ m s}^{-1}$  or less leads to an overestimate of less than 5%. The corresponding (corrected) values are 2.6 and  $1.8 \text{ m}^{-1}$  for soil and snow. Although the values themselves are not very accurate because of the scatter in the measurements and the imprecisely known path length, it can be concluded that the attenuation in both materials is quite severe.

Integrating the output from collocated vertical and horizontal geophones provides a picture of the particle motion caused by the air wave. Figure 6 shows the motion when the acoustic source was 79 m from the sensors (the same source and receiver geometry as Fig. 4). In the summer, the initial soil particle motion starting 0.2 s after the shot is down and away from the source as expected, but it almost immediately becomes retrograde<sup>16</sup> elliptical with both components about equal in size. Within 0.05 s, the horizontal component becomes much larger than the vertical component, and remains so until the motion ends. After two retrograde loops, the motion switches to prograde (at 0.25 s), then back again. It remains mostly retrograde and gradually flattens out to purely horizontal motion by 0.4 s. The maximum peak-to-peak displacements occur early in the motion, and reach  $6 \times 10^{-8} \text{ m}$  vertically and  $13 \times 10^{-8} \text{ m}$  horizontally. The final horizontal motion 0.4 s after the shot remains at about  $2 \times 10^{-8} \text{ m}$ .

In the winter, the motion also starts down and away

from the source. The motion is at first prograde and nearly all in the vertical plane. During the next 0.05 s, the motion continues to be generally prograde, but both components are about equal in size. About 0.325 s after the shot, the motion switches from prograde to retrograde, with the horizontal component being the larger one. This retrograde motion continues for two revolutions before the motion dies away. The maximum peak-to-peak displacement is  $1 \times 10^{-8} \text{ m}$  vertically and  $0.6 \times 10^{-8} \text{ m}$  horizontally.

Classically, elliptical particle motion is associated with surface waves in seismology, and this type of motion is especially clear on the winter recordings; it is the low-frequency wave following the air wave in Figs. 4 and 5. The initial vertical motion is caused by the force applied to the surface from the passage of the air wave. The prograde and retrograde motions arise from surface waves coupled to the air wave, traveling in the snow layer and in the shallow soil. Although some elliptical motion is present in the summer, most of it is rectilinear in the horizontal plane. (Rectilinear motion is usually, but not always, associated with body waves in seismology, so it cannot be used to characterize the wave type).

Figures 7 and 8 show how the air wave pulse amplitudes decayed as range increased. Least-squares fitting of the data for all of the surface vertical component geophones and for propagation ranges greater than 1 m to the equation

$$A(r) = A_1 r^{-\beta}, \quad (4)$$

where  $r$  is the distance from the source in m,  $A(r)$  is the amplitude in  $\text{m s}^{-1}$  of a vertical component geophone on the surface at range  $r$ ,  $A_1$  is a constant (the amplitude at  $r = 1 \text{ m}$ ), and  $\beta$  is the distance attenuation exponent, showed that the decay rate in the winter ( $\sim r^{-1.9}$ ) was much higher than

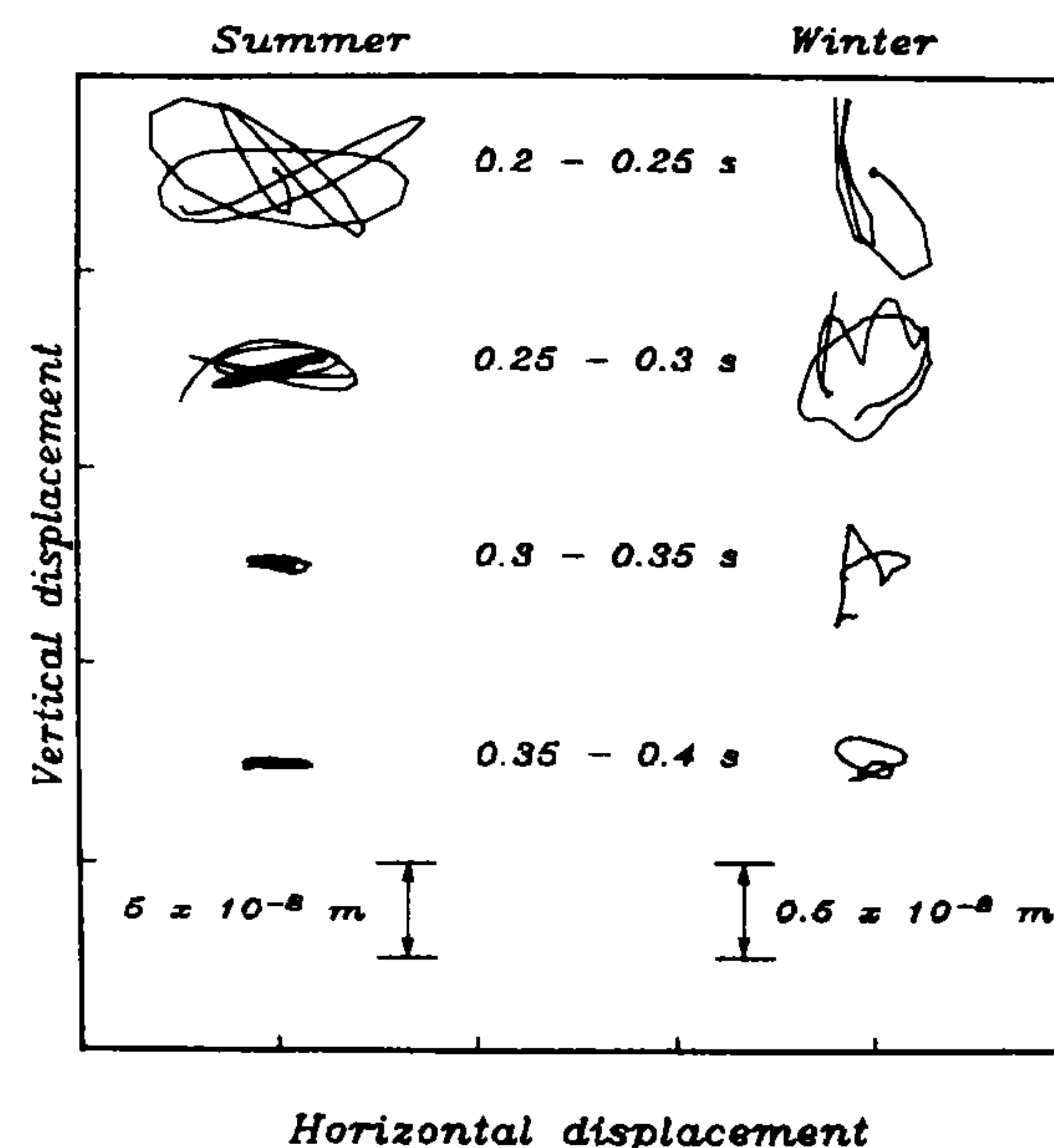


FIG. 6. Particle motion diagrams from summer and winter surface geophones at horizontal location zero (Figs. 2 and 3). The pistol was held 1 m above the surface at horizontal location 79 m east. The summer motion is in the left column; the winter motion is in the right column. From top to bottom, each segment shows a successive time interval 0.05 s long, starting 0.2 s after the pistol shot.

TABLE II. Attenuation measurements.

No. of points	$\alpha$ ( $\text{m}^{-1}$ )	95% confidence interval	Season	Material
33	3.25	1.11	summer	soil
20	1.46	1.64	winter	soil
100	1.86	0.27	winter	snow

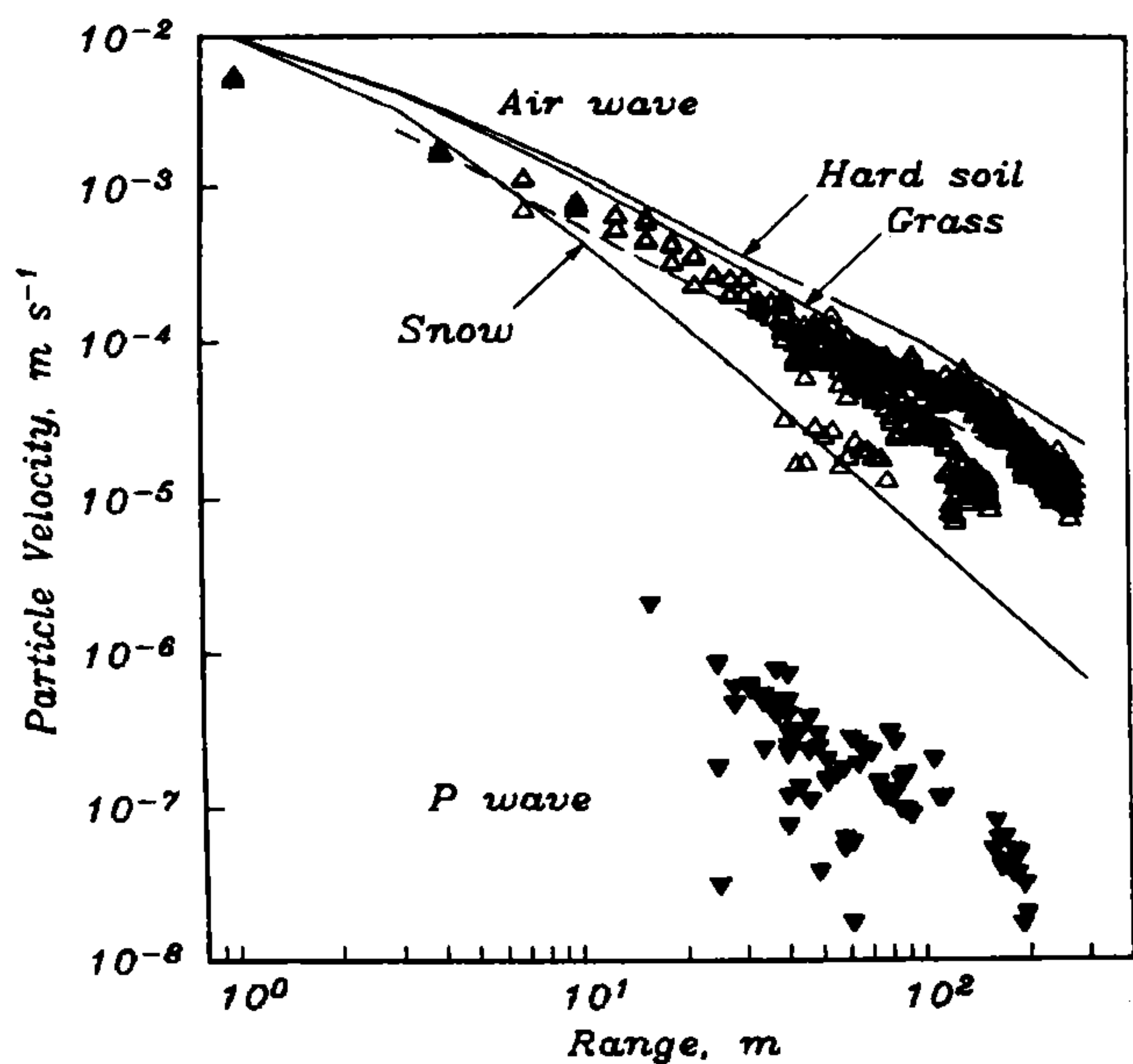


FIG. 7. Plot of first arrival amplitude versus distance from the source for vertical component geophones in the summer. Initial motion was up for the *P* waves (closed symbols) and down for the air waves (open symbols). Triangles denote amplitudes measured by receivers on the surface. A dashed line shows the least-squares fit to the air wave amplitude data used to determine the decay rate given in Table III. The solid lines are amplitudes predicted for a relatively hard soil (top), grassland (middle), and snow (bottom) using Attenborough's (1985) model.

in the summer ( $\sim r^{-1.2}$ ). A similar analysis was carried out for the microphones, but the results are not as accurate because there were fewer microphones in the array and because some of the recorded microphone waveforms were clipped, especially in the summer, and could not be used. Additional

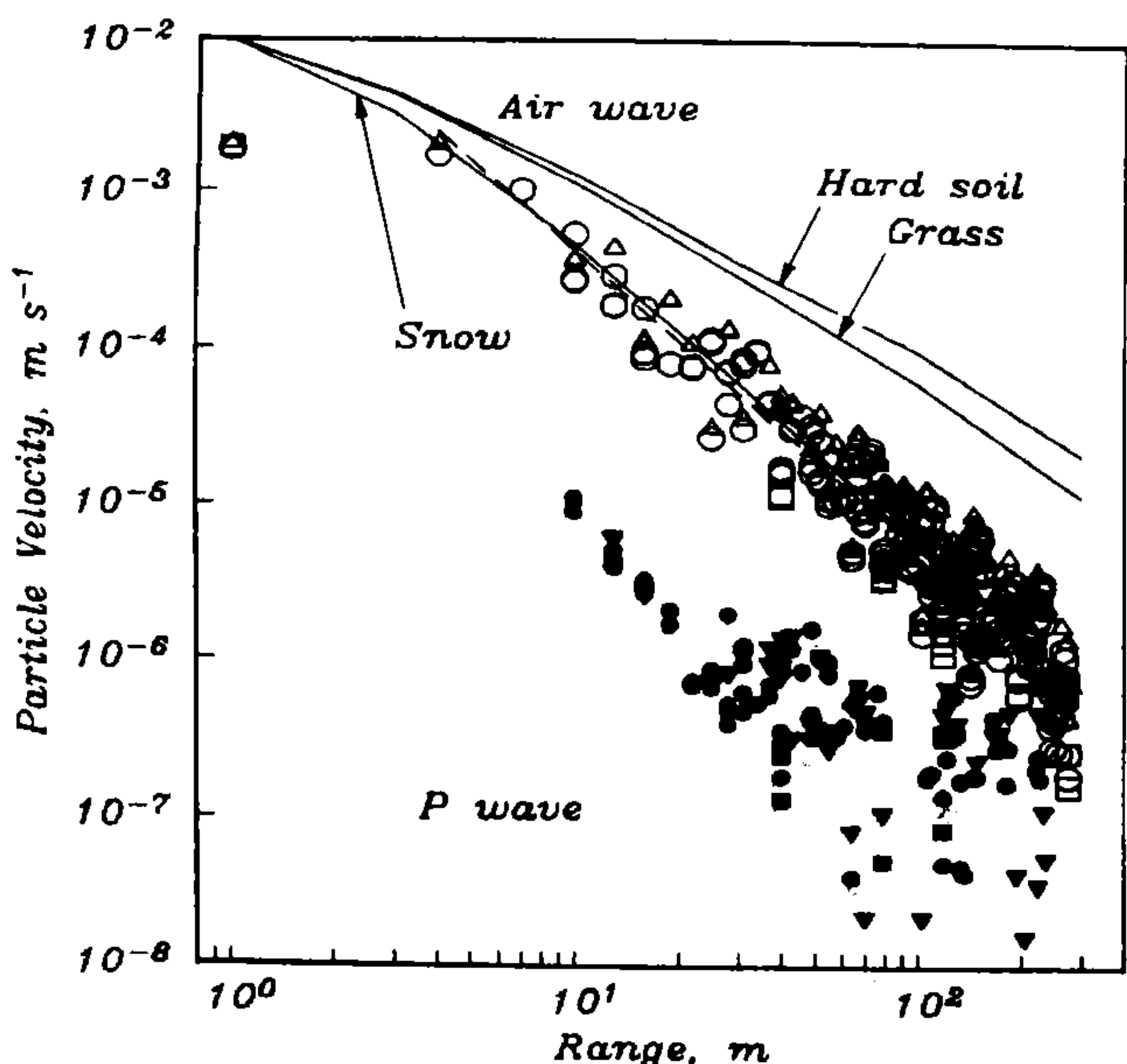


FIG. 8. Plot of first arrival amplitude versus distance from the source for vertical component geophones in the winter. Triangles, circles, and squares denote receivers at the snow surface, under the snow, and buried in the ground, respectively. Closed symbols are the *P*-wave arrivals, open symbols the air wave. A dashed line shows the least-squares fit to the air wave amplitude data used to determine the decay rate given in Table III. The predicted amplitudes (solid lines) are identical to those in Fig. 7.

details of the fit of the data to Eq. (4) are given in Table III.

There are two primary mechanisms affecting the measured decay rate: the bending of acoustic rays by the inhomogeneous atmospheric sound-speed profile and the absorption of energy by the finite impedance ground surface. For a neutral atmosphere, the sound ray paths are straight lines spreading outward evenly from the source, and the amplitude decay rate is mainly like  $r^{-1}$ . For the summer measurements, the  $3\text{-m s}^{-1}$  wind kept the atmosphere at a nearly constant temperature by mixing, and since the wind was blowing perpendicular to the propagation direction, its effect was to slightly bend the ray direction (by  $0.8^\circ$ ) and to decrease the sound velocity (by  $\sim 0.04\text{ m s}^{-1}$ ), with very little effect on the amplitude decay. The split in the air waves beyond 100 m (Fig. 7) corresponds to source locations to the west (lower amplitudes) and to the east (higher amplitudes) of the receiver array; these recordings were made on different days when atmospheric conditions may have been slightly different. In the winter, the positive temperature gradient (inversion) tended to bend upward propagating rays back down towards the ground, decreasing the amplitude decay rate and enhancing the amplitude at a given range. This gradient was about  $+2$  to  $+4\text{ }^\circ\text{C m}^{-1}$  from the surface to 2-m height, and about  $+1\text{ }^\circ\text{C m}^{-1}$  from 2 to 6 m.

The second mechanism affecting the amplitude decay rate is absorption of the airborne acoustic wave by the ground. If the ground were completely rigid, all of the rays impinging on it would be reflected back into the air without loss, and the total amplitude produced at a given range by a spherically symmetric source would be doubled by the reflection from the boundary. There has been extensive study of the effect of a ground surface with finite impedance on acoustic waves (e.g., Refs. 2, 17, and 18). Such ground conditions will increase the decay rate by absorption and transmission. Since the acoustic wave from the source propagates mainly through the atmosphere and couples locally into the ground, we calculated the decay rate of the airborne waves caused by ground absorption<sup>19</sup> for comparison with the amplitude decay measured by the geophones. Using a four-parameter model developed by Attenborough<sup>20</sup> and the Weyl-Van der Pol formulation, we determined the excess attenuation produced by the boundary at selected ranges as a function of frequency. We then integrated over the frequency bandwidth of our recording instruments to determine the effect of ground impedance on pulse amplitudes in a manner similar to that used by Don and Cramond.<sup>21</sup> Pulse amplitude decay rates for three types of ground were calculated and are plotted in Figs. 7 and 8: a relatively hard soil (with effective flow resistivity  $\sigma_e = 1820\text{ kN s m}^{-4} = 1\,820\,000\text{ N s m}^{-4}$ ), a softer soil representative of grassland ( $\sigma_e = 366$ ), and

TABLE III. Range decay for air waves.

No. of points	$\beta$	95% confidence interval	Season
458	1.17	0.09	summer geophones
352	1.89	0.15	winter geophones
66	1.31	0.59	summer microphones
142	1.52	0.45	winter microphones

snow ( $\sigma_e = 10$ ). The input parameters<sup>22</sup> for these grounds used in the calculations were taken from Attenborough<sup>20</sup> and from Attenborough and Buser.<sup>23</sup> We find that the calculated acoustic attenuation for propagation above grassland shows the same decay rate as that observed by the surface geophones in the summer, and the calculated acoustic attenuation above snow-covered ground agrees with the decay observed in the winter (Figs. 7 and 8). Our conclusion from these comparisons is that the attenuation rates measured for the air wave by the geophones in summer and winter are accounted for by differences in the ground absorption of the airborne acoustic wave. The enhancement from ray bending in the winter was not observed in the data because the absorbing effect of the ground surface, which decreased the amplitude as the range increased, was much stronger than the refraction effect.

In addition to the motion induced by the passage of the air wave from the pistol shots, earlier arrivals were also recorded by the vertical component geophones. Since these waves arrive at almost the same time as the compressional waves recorded using hammer blows, and have measured phase velocities of  $1660 \text{ m s}^{-1}$ , they must travel primarily through the ground, and penetrate at least as deep as the water table. They were strongest 40 to 80 m from the source, but were detected out as far as 230 m. This is far beyond the distance that footsteps could be detected, so these early arrivals cannot have been caused by the movement of the shooter. The decay of these waves as a function of range is also shown in Figs. 7 and 8. The above observations and synthetic seismogram modeling work indicates that these arrivals are produced by energy that couples into the ground directly beneath the source, and then travels through the subsurface as a seismic compressional ( $P$ ) wave.

These body waves are about a factor of 100 smaller in amplitude than the air waves in the summer. In the winter, the presence of the snow layer actually enhances these waves and they are only about a factor of 10 smaller than the air waves. The enhancement is caused by impedance matching that increases the transmission coefficient when snow is present. Such matching can be demonstrated by the following simple example in which we treat the ground as a purely elastic material. The plane-wave amplitude transmission coefficient at normal incidence is

$$T = (2\rho_1 c_1) / (\rho_1 c_1 + \rho_2 c_2), \quad (5)$$

where  $\rho$  and  $c$  are the density and acoustic velocity, respectively, and the subscripts refer to the upper or lower medium. With values of 0.407, 12.5, and  $369 \text{ kg m}^{-2} \text{ s}^{-1}$  for the impedances  $\rho c$  of the air, snow, and soil, the transmission coefficient from air to soil is 0.002; for air to snow to soil it is 0.004, a factor of 2 higher. Including the porosity and other details of the ground's structure would enhance the transmission coefficient of the higher porosity snow and strengthen our conclusion. The bare ground reflects acoustic waves well; the snow does not and in effect "traps" more of the incident energy.

#### IV. CONCLUSIONS

Observations have shown that an acoustic source will cause two arrivals at surface geophones or geophones buried

at shallow depths. The largest arrival is caused by the passage of the air wave, which induces a surface wave in the soil with elliptical particle motion. A 0.25-m-thick snow cover caused increased amplitude decay of the air wave, and a relative enhancement of the low-frequency air-coupled surface wave. The direction of particle motion also switched from retrograde to prograde. Under these experimental conditions, the effect of ground absorption dominates the pulse amplitudes and overrides any refractive effects of the atmosphere. Theoretical calculations of the amplitude decay of the airborne acoustic wave using Attenborough's model<sup>20</sup> are in good agreement with observations. An earlier arrival was also recorded for a body wave that traveled primarily through the subsurface, penetrating at least 4 m after coupling into the ground directly beneath the source. The body wave amplitudes increased slightly when a snow cover was introduced because of improved impedance matching.

#### ACKNOWLEDGMENTS

Thanks are given to Captain Dennis Briggs and the Vermont National Guard for supporting these experiments and coordinating our use of their firing range. Valuable assistance with the field measurements was provided by Frank Perron and especially by Steve Decato. Randy Meyer provided meteorological and snow characterization data, Rosanne Stoops analyzed the soil samples, and Matthew Pacillo provided drafting support. Keith Attenborough, Henry Bass, and James Sabatier supplied subroutines to calculate ground attenuation, and Keith Attenborough provided a manuscript<sup>23</sup> in advance of publication. Ken Jezek, Tom Landers, Malcolm Mellor, Lindamae Peck, Paul Sellmann, and Ed Wright provided useful comments or reviews. We also thank an anonymous reviewer and the Journal Editor for suggesting improvements to the paper. This work is supported by the Directorate of Research and Development, U.S. Army Corps of Engineers, Project 4A762730AT42.

<sup>1</sup>D. G. Albert, "Recent research on acoustic to seismic coupling," in *Proceedings of the DOD Symposium and Workshop on Arctic Environmental Sciences*, Laurel, MD, 27–30 January 1987 (Science and Technology Corp., Hampton, VA, 1987), pp. 223–225.

<sup>2</sup>T. F. W. Embleton, and G. A. Daigle, "Near-ground sound fields and surfaces of finite impedance," *J. Acoust. Soc. Am. Suppl. 1* **82**, S76 (1987).

<sup>3</sup>K. Attenborough, J. M. Sabatier, H. E. Bass, and L. N. Bolen, "The acoustic transfer function at the surface of a layered poroelastic soil," *J. Acoust. Soc. Am.* **79**, 1353–1358 (1986).

<sup>4</sup>H. E. Bass, L. N. Bolen, D. Cress, J. Lundien, and M. Flohr, "Coupling of airborne sound into the earth: Frequency dependence," *J. Acoust. Soc. Am.* **67**, 1502–1506 (1980).

<sup>5</sup>J. M. Sabatier, H. E. Bass, L. N. Bolen, and K. Attenborough, "Acoustically induced seismic waves," *J. Acoust. Soc. Am.* **80**, 646–649 (1986).

<sup>6</sup>J. M. Sabatier, H. E. Bass, L. N. Bolen, K. Attenborough, and V. V. S. Sastry, "The interaction of airborne sound with the porous ground: The theoretical formulation," *J. Acoust. Soc. Am.* **79**, 1345–1352 (1986).

<sup>7</sup>J. M. Sabatier, H. E. Bass, and G. R. Elliott, "On the location of frequencies of maximum acoustic-to-seismic coupling," *J. Acoust. Soc. Am.* **80**, 1200–1202 (1986).

<sup>8</sup>A. Gudesen, "Air to ground coupling on a sandy soil in northwest Germany," in *Proceedings of the Second Symposium on Long Range Sound Propagation and Seismic/Acoustic Coupling*, New Orleans, LA, 13–16 February 1985, edited by H. E. Bass and K. Attenborough (University of Mississippi, Oxford, MS, 1985), pp. 405–423.

- <sup>9</sup>H. van Hoof, "Acoustic/seismic measurements in the Netherlands," in *Proceedings of the Second Symposium on Long Range Sound Propagation and Seismic/Acoustic Coupling*, New Orleans, LA, 13–16 February 1985, edited by H.E. Bass and K. Attenborough (University of Mississippi, Oxford, MS, 1985), pp. 453–463.
- <sup>10</sup>R. W. Knapp, "Observations of the air-coupled wave as a function of depth," *Geophysics* **51**, 1853–1857 (1986).
- <sup>11</sup>D. G. Albert, "The effect of snow on vehicle-generated seismic signatures," *J. Acoust. Soc. Am.* **81**, 881–887 (1987).
- <sup>12</sup>L. Peck, "Acoustic-to-seismic coupling through a snow layer," in *Proceedings of SNOW Symposium IV*, Hanover, NH, August 1986, edited by A. W. Hogan and R. Redfield (USA CRREL Special Rep. 87-12, Hanover, NH, 1987), pp. 47–55 (available from Defense Technical Information Center, Alexandria, VA 22314, order No. ADB115486).
- <sup>13</sup>D. P. Stewart and P. McClintock, *Surficial geologic map of Vermont* (Vermont Geological Survey, Montpelier, VT, 1970), scale 1:250,000.
- <sup>14</sup>C. G. Doll, W. M. Cady, J. B. Thompson, Jr., and M. P. Billings, *Centennial geologic map of Vermont* (Vermont Geological Survey, Montpelier, VT, 1970), scale 1:250,000.
- <sup>15</sup>H. A. J. M. van Hoof and K. W. F. M. Doorman, "Coupling of airborne sound in a sandy soil" (Netherlands Organization for Applied Scientific Research, Laboratory for Electronic Developments for the Armed Forces, Oegstgeest, NL, 1983) TNO/LEOK Rep. No. TR 1983-09.
- <sup>16</sup>Retrograde motion is opposite in direction to the motion of a point on the surface of a disk that is rolling along the ground from the source to the receiver.
- <sup>17</sup>T. F. W. Embleton, J. E. Piercy, and N. Olson, "Outdoor sound propagation over ground of finite impedance," *J. Acoust. Soc. Am.* **59**, 267–277 (1976).
- <sup>18</sup>J. Nicolas, J.-L. Berry, and G. A. Daigle, "Propagation of sound above a finite layer of snow," *J. Acoust. Soc. Am.* **77**, 67–73 (1985).
- <sup>19</sup>Further details of the method used to calculate the ground absorption are included in D. G. Albert and J.A. Orcutt, "Acoustic pulse propagation above grassland and snow: Comparison of theoretical and experimental waveforms," submitted to *J. Acoust. Soc. Am.*
- <sup>20</sup>K. Attenborough, "Acoustical impedance models for outdoor ground surfaces," *J. Sound Vib.* **99**, 521–544 (1985).
- <sup>21</sup>C. G. Don and A. J. Cramond, "Impulse propagation in a neutral atmosphere," *J. Acoust. Soc. Am.* **81**, 1341–1349 (1987).
- <sup>22</sup>The input parameters required for the four-parameter model are the flow resistivity  $\sigma_c$ , porosity  $\Omega$ , pore shape factor ratio  $s_f$ , and grain shape factor  $n'$  (see Attenborough<sup>20</sup> for the definition of the latter two parameters). For all of the calculations, we set  $n' = 0.5$ . For the hard soil, the other input parameters were  $\sigma_c = 1820 \text{ kN s m}^{-4}$ ,  $\Omega = 0.38$ , and  $s_f = 0.73$ . For grass, we used  $\sigma_c = 366$ ,  $\Omega = 0.27$ , and  $s_f = 0.73$ . For snow, we used  $\sigma_c = 10$ ,  $\Omega = 0.60$ , and  $s_f = 0.50$ . This layer was 0.25 m thick, and was over a soil layer with the parameters  $\sigma_c = 300$ ,  $\Omega = 0.40$ , and  $s_f = 0.75$ .
- <sup>23</sup>K. Attenborough and O. Buser, "On the application of rigid-porous models to impedance data for snow," *J. Sound Vib.* **124**, 315–327 (1988).